Sensors & Actuators: B. Chemical 367 (2022) 132034

Contents lists available at ScienceDirect

Sensors and Actuators: B. Chemical

journal homepage: www.elsevier.com/locate/snb

Cobalt ion doping to improve electrochemiluminescence emisssion of gold nanoclusters for sensitive NIR biosensing

Hongying Jia [a], Lei Yang [a], Dawei Fan [a], Xuan Kuang [a], Xu Sun [a], Qin Wei [a,*], Huangxian Ju [a,b,**]

[a] Collaborative Innovation Center for Green Chemical Manufacturing and Accurate Detection, School of Chemistry and Chemical Engineering, University of Jinan, Jinan 250022, PR China

[b] State Key Laboratory of Analytical Chemistry for Life Science, School of Chemistry and Chemical Engineering, Nanjing University, Nanjing 210023, PR China

ARTICLE INFO

Keywords:
Luminophores
Au nanoclusters
Electrochemiluminescence
Near-infrared
Biosensing
Immunosensing

ABSTRACT

Screening highly efficient luminophores has attracted considerable attention in bioanalysis. To improve the emission efficiency of nanoclusters (NCs), this work designed an ion doping strategy for regulating the electcrochemiluminesent (ECL) emisssion of gold nanoclusters (AuNCs). This strategy could be conveniently performed by doping cobalt ions (Co^{2+}) in cysteamine and N-acetyl-L-cysteine stabilized AuNCs, which not only generated tunable hole-injection channels for the ECL emission, but also reduced the superficial defects to promote electron transfer through the synergetic effect of Au and Co^{2+}. The obtained Co^{2+}-AuNCs displayed 0.2 V lower anodic emission potential and double ECL efficiency and intensity in the near-infrared region (NIR) compared to the AuNCs. Benefitting from the enhanced NIR ECL emission and the excellent biocompatibility of Co^{2+}-AuNCs, as well as the lowered background interference, a sensitive "signal-on" immunosensor using neuron specific enolase (NSE) as a model analyte was proposed. This ECL biosensing method showed a limit of detection (LOD) of 0.16 fg/mL (S/N = 3), a linear range from 0.5 fg/mL to 1 ng/mL, excellent specificity and good practicability, demonstrating the excellent ECL performance of Co^{2+}-AuNCs in bioanalysis. This work provides a way to modulate the ECL features of NCs-based luminophores and improve the performance of ECL bioassay.

1. Introduction

Electrochemiluminescence (ECL) is an electrochemically triggered radiative electron transfer process [1–4], and has been extensively employed in bioassays owing to its intrinsically low background, high sensitivity, broad detection range, and favorable controllability [5–7]. Both enhanced ECL response and lowered triggering potential are overwhelmingly conducted as the popular exploration for ECL bioassays, because normal ECL bioassays are usually accompanied by the concerns of electrode compatibility and electrochemical interference resulted from high triggering potential for ECL of normal luminophores [8]. In addition, efficient near-infrared (NIR) ECL assay with a low triggering potential is also intensively anticipated as a promising alternative to the traditonal ECL assay in eye-visible region with different luminophores, such as luminol [9], ruthenium complex [10], polymer dots (Pdots) [11] and semiconductor nanocrystals [12]. Thus, screening promising ECL luminophores to enable NIR ECL assay with low triggering potential, efficient ECL response and negligibly biotoxic concern is of great significance for the ECL evolution.

Over the past few years, metal nanoclusters (NCs), especially the gold nanoclusters (AuNCs) [13], have been exploited as a kind of prospective ECL luminophores for the detection of protein [14], microRNAs [15], and small moleculars [16] due to their unique chemicophysical characteristics, good biocompatibility, low biotoxic nature and tunable luminescent features. Although diverse AuNCs have been used as the ECL luminophores, the high triggering potential and the limited ECL efficiency (Φ_{ECL}) that is owing to the depressed charge transfer in electrogenerated procedure and increased non-radiative transition in the energy relaxation procedure are still the main stumbling blocks for the extensive application of AuNCs-related ECL [17–19]. Fortunately, some instructional research has proved that the Φ_{ECL} and emission waveband of AuNCs can be adjustable via treating the AuNCs with a serials strategies. The ehanced Φ_{ECL} of AuNCs via electrochemical reduction [17] or aggregation-induced emission (AIE) [20], and the

* Corresponding author.
** Corresponding author at: Collaborative Innovation Center for Green Chemical Manufacturing and Accurate Detection, School of Chemistry and Chemical Engineering, University of Jinan, Jinan 250022, PR China.
E-mail addresses: sdjndxwq@163.com (Q. Wei), hxju@nju.edu.cn (H. Ju).

https://doi.org/10.1016/j.snb.2022.132034
Received 14 February 2022; Received in revised form 2 May 2022; Accepted 11 May 2022
Available online 17 May 2022

efficient emission by forming host-guest assemblies around the AuNCs luminophores have been realized [21]. Meanwhile, the controllable ECL wavelength of AuNCs has also been confirmed through altering the ligand impacts [22]. More promisingly, Zou has further demonstrated that AuNCs can be incorporated with another metal ion to form bimetallic NCs (BNCs), and the synergetic influence of the metal elements result in the promoted ECL response as well as changed charge-recombine route [23]. The incorporation of transition metals in AuNCs can change the electronic structure, and enhance the optical properties and synthetic controllability [24]. Especially, the incorporation of cobalt leads to good catalytic activity and enhanced quantum yield [25,26]. These researches on the ECL of AuNCs mainly focus on the enhanced Φ_{ECL} inside visible region. In this work, a cobalt ion (Co^{2+}) doping strategy was designed to achieve regulable ECL wavelength, while led to enhanced NIR ECL emission.

The doping of Co^{2+} in cysteamine and N-acetyl-L-cysteine stabilized AuNCs not only generated tunable hole-injection channels for the ECL emission, but also reduced the superficial defects of AuNCs to promote electron transfer. The obtained Co^{2+}-AuNCs showed 0.2 V lower anodic emission potential and double ECL efficiency and intensity in NIR region with triethylamine (TEA) as a coreactant, compared to the AuNCs. In view of the superiorities and the excellent biocompatibility of Co^{2+}-AuNCs, as well as the low background interfernce of NIR ECL emission, a promising"signal-on" NIR ECL immunoassay strategy was proposed with Co^{2+}-AuNCs as the labeling tag and neuron specific enolase (NSE) as the model analyte (Scheme 1). NSE is a perfect biomarker for the diagnosis of small cell lung carcinoma (SCLC) with a cut-off value of 12 ng/mL in serum samples [27]. The serum NSE concentrations of most SCLC patients are between 12.5 ng/mL and 25 ng/mL [28,29]. The immunosensing strategy exhibited good linearity in a wide concentration range, a limit of detection down to 0.16 fg/mL (S/N = 3), acceptable accuracy and excellent specificity, demonstrating the excellent ECL performance of Co^{2+}-AuNCs in bioanalysis. This work supplies a new way to modulate the ECL features of NCs-based luminophores and a novel ECL luminophore with admirable performance for bioassay.

2. Experimental

2.1. Chemicals, materials and apparatus

Detailed information about chemicals, materials and apparatus applied in this work are displayed in the Supporting Information.

2.2. Preparation of Co^{2+}-AuNCs

All relevant glasswares used in the following experiments were cleaned with HNO_3-HCl (1:3, v/v), washed with ultrapure water and ethanol, and dried for the subsequent use. The preparation of Co^{2+}-AuNCs was synthesized via the preceding reported process with certain modifications [30]. In brief, cysteamine (Cys, 30 mmol/L, 0.75 mL), N-acetyl-L-cysteine (NAC, 30 mmol/L, 0.25 mL), $HAuCl_4.3\ H_2O$ (25 mmol/L, 1 mL) and 1 mL $CoCl_2$ aqueous solution with varied concentrations (25, 12.5 or 6.25 mmol/L) were added into 7 mL ultrapure water to incubate at 90 °C for 90 min (Scheme 1A). As control, the precursor at the Au/Co molar ratios of 1:0 and 0:1 were utilized to prepare the monometallic AuNCs and CoNCs, respectively. After the reaction, the supernatant was collected by centrifuging the mixture, and the precipitate was discarded. Finally, the precipitate was obtained by centrifugation with isopropyl alcohol at 15,000 rpm for three times, and dissolved in the ultrapure water to form 1 mg/mL AuNCs, CoNCs and Co^{2+}-AuNCs, respectively, which were held at 4 °C.

2.3. Preparation of $Ab_2|Co^{2+}$-AuNCs

The preparation of Co^{2+}-AuNCs labeled signal antibody (Ab_2) (i.e., $Ab_2|Co^{2+}$-AuNCs) was shown in Scheme 1A [22]. Firstly, Co^{2+}-AuNCs (1 mg/mL, 1 mL) were blended with 1-ethyl-3-(3-dimethyl-amino--propyl) carbodiimide hydrochloride (EDC) (0.10 mol/L, 100 μL), *N*-hydroxysuccinimide (NHS) (0.10 mol/L, 100 μL) to react for 30 min at room temperature (RT) for activating the carboxyl groups of Co^{2+}-AuNCs. The activated Co^{2+}-AuNCs were then purified by

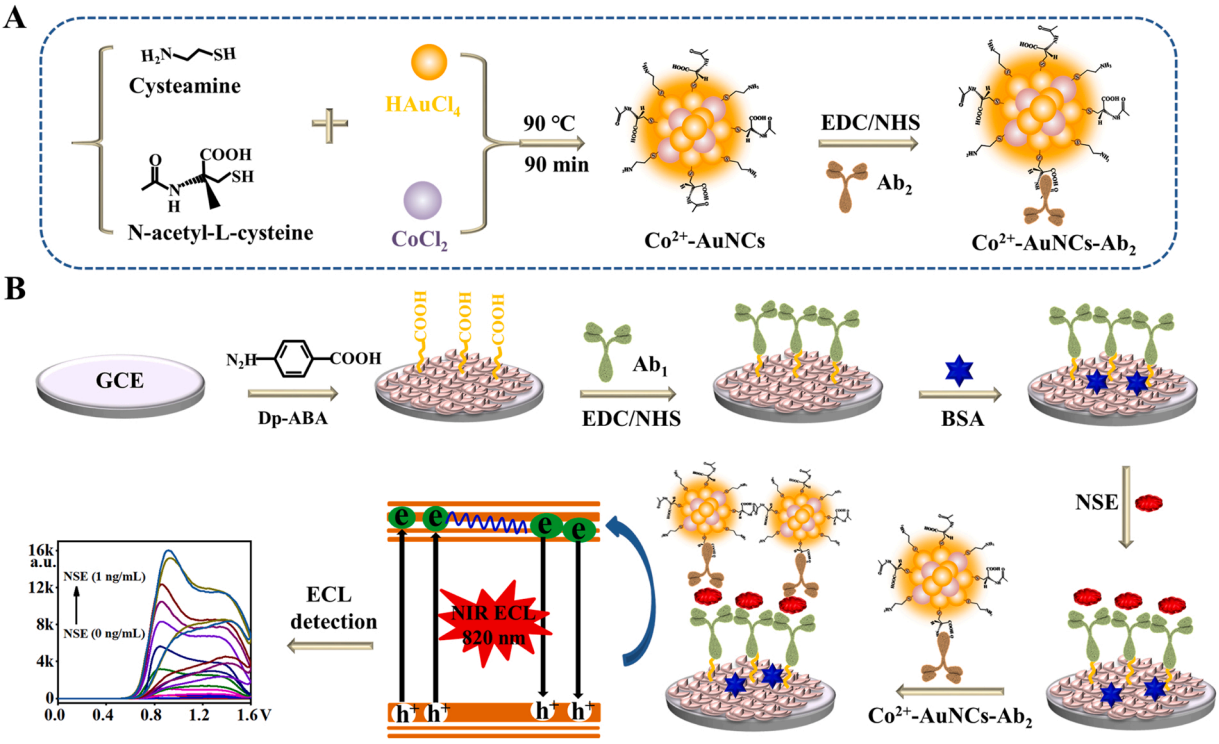

Scheme 1. Schematic illustration for (A) preparation of $Ab_2|Co^{2+}$-AuNCs, and (B) fabrication of immunosensor and NIR ECL immunoassay with Co^{2+}-AuNCs as ECL tag.

centrifugation and incubated with Ab_2 solution (100 μg/mL, 1 mL) under the condition of shaking at RT for 8 h. The mixture was centrifugated at 8,000 rpm for 15 min and redissolved in 0.1 mol/L pH 7.4 phosphate buffer solution (PBS) containing bovine serum albumin (BSA) (0.1%, 100 μL) for 1 h to block the uncombined binding sites. Finally, the as-obtained $Ab_2|Co^{2+}$-AuNCs conjugate was rinsed with 0.10 mol/L pH 7.4 PBS for three times and dispersed in 1 mL 0.10 mol/L pH 7.4 PBS at 4 °C.

2.4. Fabrication of Co^{2+}-AuNCs modified GCE and immunosensor

Co^{2+}-AuNCs modified GCE was obtained by coating a drop of 10 μL 1 mg/mL Co^{2+}-AuNCs dispersion on the GCE and drying under infrared radiation.

The fabrication chart of the NIR ECL immunosensor was exhibited in Scheme 1B. At first, glassy carbon electrode (GCE) was immersed into 0.1 mol/L pH 7.4 PBS containing 5 mmol/L p-aminobenzoic acid (ABA) to scan the potential between 0.40 and 1.20 V at 10 mV/s for two cycles for depositing ABA monolayer (Dp-ABA) on the surface of GCE [31]. The activation of carboxyl groups of GCE=ABA was achieved by dropping EDC (0.5 mol/L, 10 μL) and NHS (0.5 mol/L, 10 μL) on the surface for 30 min, which were then covalently bound with capture antibody (Ab_1) (10 μg/mL, 10 μL) for 2 h. The obtained GCE=ABA-Ab_1 was rinsed with PBS and incubated with BSA to block the unspecific active binding sites to obtain the immunosensor, named as GCE=ABA-Ab_1.

2.5. Immunoassay

The NIR ECL immunosensing was performed by incubating the NSE immunosensor with 10 μL of NSE at different contents at RT for 2 h to acquire the GCE=ABA-Ab_1 <NSE, and then with $Ab_2|Co^{2+}$-AuNCs bioconjugate for another 1 h to form GCE=ABA-Ab_1 <NSE>$Ab_2|Co^{2+}$-AuNCs. Afterward, the sandwiched immunosensor was applied for ECL measurement in 0.1 mol/L pH 7.4 PBS with 0.1 mol/L TEA by scanning the potential between 0 and + 1.6 V at 50 mV/s.

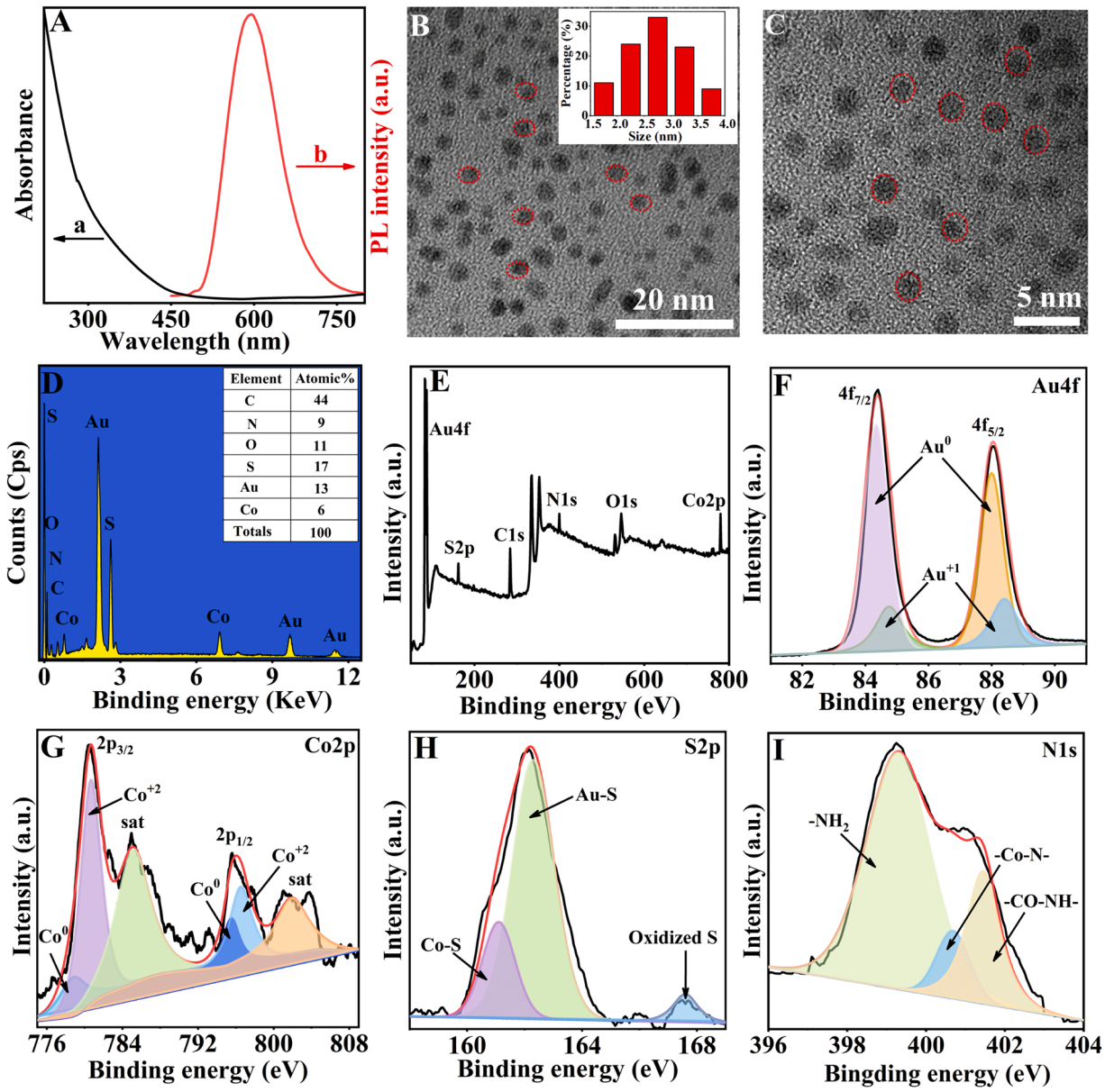

Fig. 1. . (A) UV–vis absorption (a) and PL spectra (b), (B, C) TEM images, (D) EDS pattern, (E) XPS survey spectrum of Co^{2+}-AuNC. (F-I) XPS spectra of Co^{2+}-AuNC in (F) Au4f, (G) Co2p, (H) S2p and (I) N1s regions. Inset of B: corresponding size distribution of Co^{2+}-AuNC.

3. Results and discussion

3.1. Characterizations of Co^{2+}-AuNCs, AuNCs and CoNCs

The Co^{2+}-AuNCs demonstrated featureless UV–vis absorption spectrum (Fig. 1A, curve a) and monochromatic photoluminescence (PL) with maximum emission at 595 nm as well as full width at half-maximum (FWHM) of around 100 nm (Fig. 1A, curve b). Meanwhile, the Co^{2+}-AuNCs with different Au/Co molar ratios also exhibited featureless UV–vis absorption (Fig. S1, curve a-d), and the CoNCs exhibited much weaker absorption in comparison to that of Co^{2+}-AuNCs (Fig. S1, curve e). In addition, the PL emission of Co^{2+}-AuNCs with different Au/Co molar ratios occurred at the same wavelength (Fig. S2), but the PL intensitity was related to the Au/Co molar ratio, and the maximum PL intensity of Co^{2+}-AuNCs occurred at the Au:Co of 2:1 (Fig. S2, curve c). These results indicated that the heteroatomic Co could bright out enhanced optical properties via passivating the surface defects and inhibiting the non-radiative recombination of AuNCs [32]. Furthermore, no PL was obtained under the absence of Au element (Fig. S2, curve e), which meant that it was difficult to yield luminescent signal for CoNCs with and Cys and NAC as the capping agents.

The average particle size of spherical Co^{2+}-AuNCs at Au:Co of 2:1 was determined as 2.7 nm (Fig. 1B and Fig. 1C), which was larger than that of spherical AuNCs with a dimension around 2.3 nm (Fig. S3), indicating that the Co^{2+} involved doping strategy affected on the size. The energy dispersive spectroscopic (EDS) pattern of the Co^{2+}-AuNCs exhibited evident peaks for Au and Co with molar ratio of 13:6, and some peaks belonged to Co element (Fig. 1D), which confirmed that Co was doped into the AuNCs via the doping method [26].

The elemental composition of Co^{2+}-AuNCs was demonstrated by X-ray photoelectron spectroscopy (XPS). Then, the XPS survey spectra (Fig. 1E) of Co^{2+}-AuNCs specified the presence of Au4f, Co2p, S2p and N1s (Fig. 1F-I). The Au4f spectrum showed four peaks at 84.3, 84.7, 87.9 and 88.4 eV. The $Au4f_{7/2}$ (84.3 eV) and $Au4f_{5/2}$ (87.9 eV) signals were belonged to Au(0), and the $Au4f_{5/2}$ (88.4 eV) and $Au4f_{7/2}$ (84.7 eV) signals were indexed to of Au(I) [33]. The slight Au(I) attached to the surface of Au(0) core was utilized for stabilizing the Au(0), because the resulting Au(I) could obtain a protective shell to connect with the thiolate sulfur atoms [34]. Six separate peaks were observed in the Co2p region, which certified the presence of Co element. The peaks located at 794.9 eV and 778.8 eV were regarded as the $2p_{1/2}$ and $2p_{3/2}$ spin states of Co(0), meanwhile the composition at 780.6 and 796.4 eV was belonged to the Co in the groups of Co–N and Co–O [35]. Furthermore, the peaks centered at 784.2 and 801.9 eV were distributed to the divalent Co(II) located on the surface of Co^{2+}-AuNCs, which indicated that the configurational ions of Co^{2+} had been appeared onto the Co^{2+}-AuNCs surface [26]. In total, the Co^{2+}-AuNCs presented the thiolate-capped core-shell nanostructures of Au(0)Co(0)@Co(II)Au(I) [36].

The spectrum of S could be further decomposed into three different peaks (Fig. 1H). The peak at 161.6 eV was associated with the Co–S group, and the peak situated at 163.4 eV was the Au–S group [22,35]. The N1s spectrum showed three peaks distinctly (Fig. 1I). The peaks located at 399.6 eV was corresponded to the $–NH_2$ groups, the peaks located at 401.3 eV was associated with the –Co–NH– group, and the peak at 400.2 eV was originated from the group of –Co–N– [26]. The XPS analysis demonstrated that Co^{2+} was successfully doped onto the AuNCs, and NAC and Cys were also modified on Co^{2+}-AuNCs.

3.2. Electrochemical and coreactant ECL properties of Co^{2+}-AuNCs

In 0.1 mol/L pH 7.4 PBS containing 0.1 mol/L TEA, the GCE showed the electrochemically oxidation peak of TEA with an onset potential of + 0.5 V (Fig. 2A, curve a). After deprotonation of the oxidation product, an intensive reducing radical species $TEA^{\bullet}$ could be produced for injecting electrons onto the hole-injected states of oxidized NCs (inset of Fig. 2A), Co^{2+}-$AuNCs^{\bullet+}$ or $AuNCs^{\bullet+}$ (Fig. 2A, curves b-e), which brought efficient ECL emission from NCs (Fig. 2B, curves b-e) [20]. It was obvious that the Co^{2+}-AuNCs modified electrode at Au:Co of 2:1 exhibited the largest cyclic voltammetry (CV) peak current and the

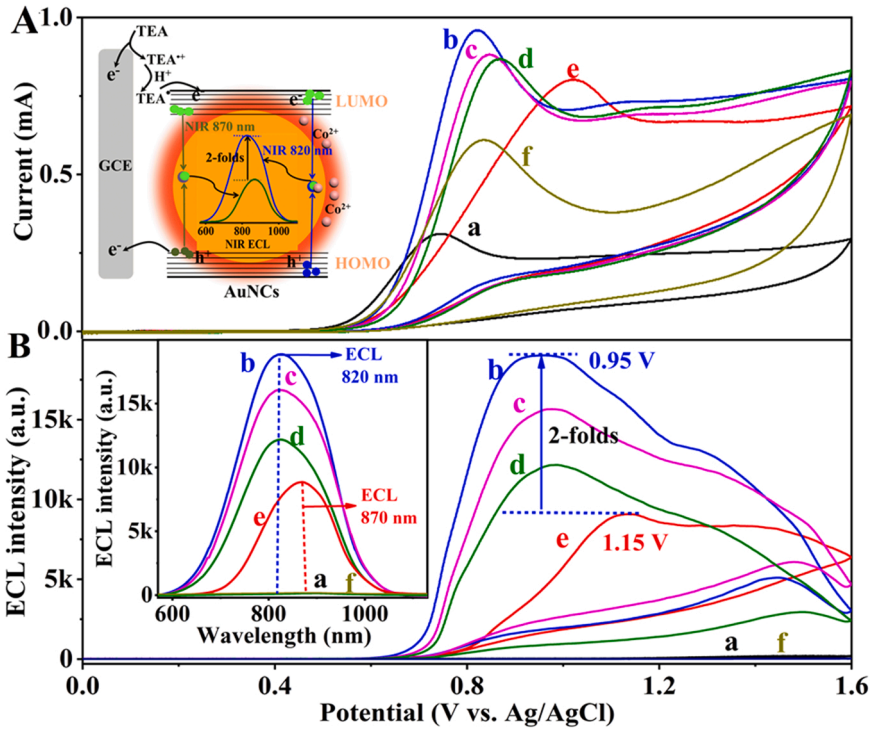

Fig. 2. . (A) CV and (B) ECL-potential profiles of (a) bare GCE, (b-d) Co^{2+}-AuNC modified GCE with Au:Co molar ratio of 2:1 (b), 4:1 (c) and 1:1 (d), (e) AuNCs modified GCE and (f) CoNCs modified GCE and in 0.1 mol/L pH 7.4 PBS containing 0.1 mol/L TEA via scanning the potential from 0 to + 1.6 V at 50 mV/s. Inset of A: schematic illustration for the blue-shifted ECL of AuNCs via Co^{2+} related doping strategy and B: corresponding accumulated ECL spectra.

lowest oxidation potential (Fig. 2A, curve b), which also led to the strongest ECL peak at + 0.95 V (Fig. 2B, curve b). The increasing peak current upon the change of working electrodes in Fig. 2A (curves b-d) was coresponding to typical electrocatalytic oxidation process of Co^{2+}-AuNCs mediated by TEA [20]. Different from + 1.15 V of AuNCs modified GCE (Fig. 2B, curve e), the ECL peaks of Co^{2+}-AuNCs modified GCEs at all Au:Co values occurred at + 0.95 V (Fig. 2B, curves b-d), implying that AuNCs and Co^{2+}-AuNCs presented different hole-injected channels for ECL emission [37]. The enhanced ECL intensity of Co^{2+}-AuNCs compared with AuNCs might be concerned with the synergetic consequences from the Au and Co as well as the catalytic performance of Co^{2+} [38]. In addition, although CoNCs modified GCE also showed the enhanced peak current as seen at Co^{2+}-AuNCs modified electrode (Fig. 2B), it did not show the ECL emission (Fig. 2B, curve f), indicating that the CoNCs could not supplied as an ECL luminophore.

The ECL emssion of Co^{2+}-AuNCs modified electrodes at all Au:Co ratios occurred at 820 nm (inset of Fig. 2B, curves b-d), 50 nm blue-shift compared with AuNCs (curve e). Considering that the ECL emission was attributed to the hole-electron recombination on the NCs surface [39], the presence of Co in the AuNCs led to changed surface state to affect the recombination energy (inset of Fig. 2A).

3.3. DPV profiles of Co^{2+}-AuNCs, AuNCs and CoNCs modified electrodes

To better understand the electrochemical behaviours of the NCs, differential pulse voltammetry (DPV) was performed to examine their cathodic and anodic processes. The AuNCs and CoNCs exhibited the respective reduction peaks at − 1.27 and − 1.11 V (Fig. 3A, Red_1 in curve b and Red_2 in curve c), which indicated that they were electrochemically injected electrons at the cathodic potentials. In addition, the Co^{2+}-AuNCs displayed two well-defined reductive peaks at − 1.27 and − 1.11 V (Fig. 3A, curve d). Thus the introduction of Co^{2+} into AuNCs led to two electron-injecting processes with the peak spacing of 0.16 V. In the reversed scanning from 0 to + 1.6 V, the AuNCs and CoNCs displayed the oxidation peaks at + 0.87 and + 1.21 V (Fig. 3B, Ox_1 in curve b and Ox_2 in curve c), respectively, which demonstrated that both AuNCs and CoNCs were electrochemically oxidized to form injecting holes. The Co^{2+}-AuNCs exhibited two oxidation peaks at + 0.87 and + 1.21 V (Fig. 3B, curve d), which indicated two hole-injecting processes with the peak spacing of 0.34 V. Compared with the AuNCs, the two oxidation peaks of Co^{2+}-AuNCs meant that the doping of Co element changed the hole-injection channel and promoted the electron transfer.

3.4. Annihilation ECL behaviors of AuNCs and Co^{2+}-AuNCs

In N_2-saturated 0.1 mol/L pH 7.4 PBS, the oxidative and reductive states of AuNCs could be obtained by setting the potential from + 0.87 to − 1.27 V for 1 s, which led to quite weak annihilation ECL emission (Fig. S4A). Meanwhile, almost no annihilation ECL emission for AuNCs was observed in setting the potential from − 1.27 V to + 0.87 V (Fig. S4B), indicating the oxidative species of AuNCs was more stable than the reductive species for ECL [21]. After doping Co element in NCs, the Co^{2+}-AuNCs exhibited obvious annihilation ECL response in setting the potential both from + 0.87 to − 1.27 V and from − 1.27 to − 0.87 V (Fig. 4), indicating that the Co^{2+} doping enhanced the annihilation ECL via the corresponding synergetic effect. Moreover, two electron-injecting processes at − 1.11 and − 1.27 V and two hole-injecting processes at + 0.87 V and + 1.21 V also showed the ECL emission for Co^{2+}-AuNCs. Obviously, the achieved annihilation ECL for the process from the electron-injecting to the hole-injecting was stronger (Fig. 4E-4 H) than that in reversed stepping (Fig. 4A-4D), indicating that the reductive form of Co^{2+}-AuNCs was more stable than the oxidative form.

3.5. Coreactant ECL behaviors and mechanism of Co^{2+}-AuNCs

Considering the deprotonation of the oxidation product of coreactant to produce $TEA^{\bullet}$, the pH effect of detection solution on ECL response was firstly examined with Co^{2+}-AuNCs at Au:Co of 2:1, which was used in all following experiments. With the increasing pH from 5.5 to 8.5, the ECL response enhanced and reached the maximum at pH 8.0 (Fig. 5 A). Thus pH 8.0 was adopted as the optimal pH (Fig. 5 A), at which the produced $TEA^{\bullet}$ could give electron to oxidized Co^{2+}-AuNCs to produce excited Co^{2+}-AuNCs* for the ECL emission. The ECL mechanism could be described as follows:

$$TEA \rightarrow TEA^{\bullet+} + e^{-} \quad (1)$$

$$TEA^{\bullet+} \rightarrow TEA^{\bullet} + H^{+} \quad (2)$$

$$Co^{2+}\text{-AuNCs} \rightarrow Co^{2+}\text{-AuNCs}^{\bullet+} + e^{-} \quad (3)$$

$$Co^{2+}\text{-AuNCs}^{\bullet+} + TEA^{\bullet} \rightarrow Co^{2+}\text{ - AuNCs*} \quad (4)$$

$$Co^{2+}\text{-AuNCs*} \rightarrow Co^{2+}\text{-AuNCs} + h\nu \quad (5)$$

The coreactant greatly affects the ECL emission. Thus other coreactants such as triethanolamine (TEOA), tripropylamine (TprA), N-butyldiethanolamine (BDTA), hydrazine hydrate solution (N_2H_4) and hydrogen peroxide (H_2O_2) were examined. As shown in Fig. 5B, TEA was the optimum coreactant. Its optimum concentration should be 0.1 mol/L (Fig. 5C), at which the ECL response reached the maxmium with the scanning rate of 50 mV/s (Fig. 5D).

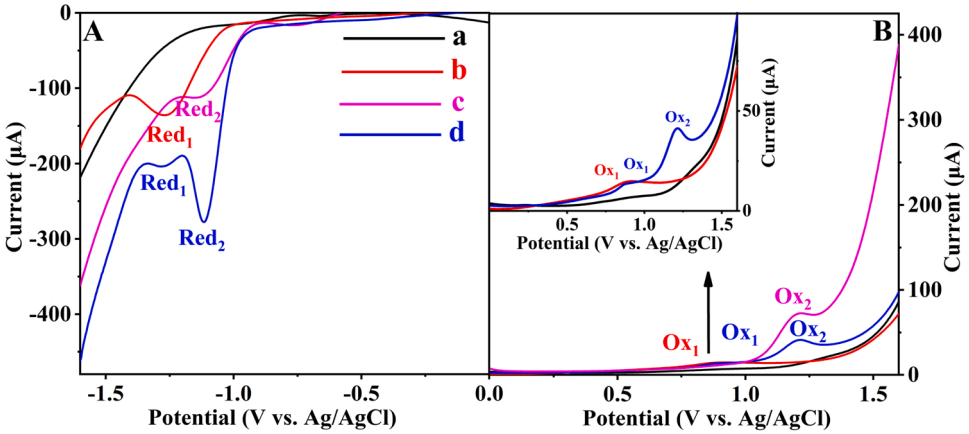

Fig. 3. . (A) Cathodic and (B) anodic DPV curves of (a) GCE, and (b) AuNCs, (c) CoNCs and (d) Co^{2+}-AuNCs modified GCE in N_2-saturated 0.1 mol/L pH 7.4 PBS.

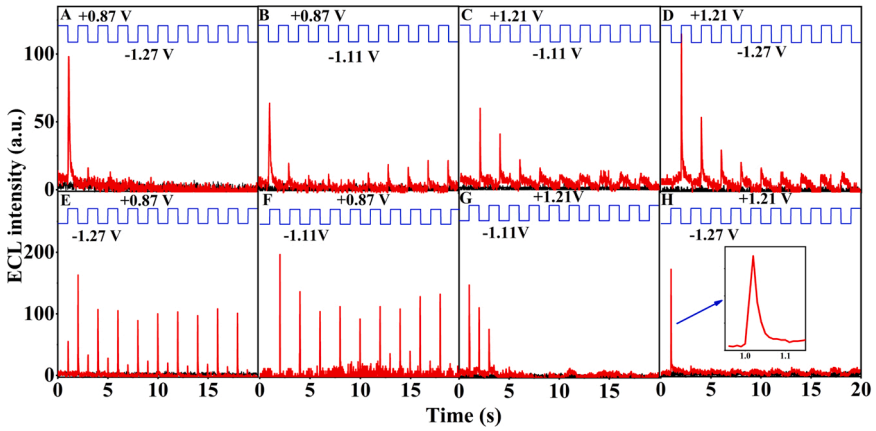

Fig. 4. ECL transients of GCE and Co^{2+}-AuNCs modified GCE in N_2-saturated 0.1 mol/L pH 7.4 PBS by steppingthe potential from (A) + 0.87 to − 1.27 V, (B) + 0.87 to − 1.11 V, (C) + 1.21 to − 1.11 V, (D) + 1.21 to − 1.27 V, (E) − 1.27 to + 0.87 V, (F) − 1.11 to + 0.87 V, (G) − 1.11 to + 1.21 V and (H) − 1.27 to + 1.21 V at 1 Hz. The blue line represents the applied potential steps.

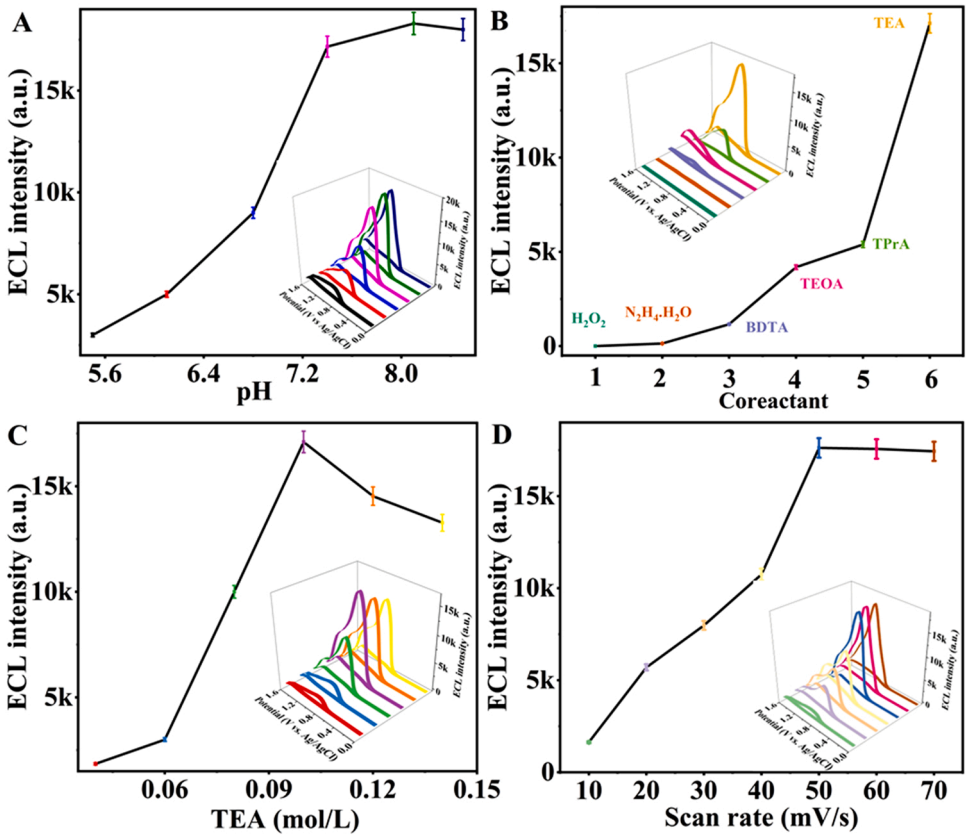

Fig. 5. . (A) Effects of pH, (B) coreactant (marked in different colors) at 0.1 mol/L, (C) TEA concentration and (D) scan rate on ECL intensity of Co^{2+}-AuNCs modified GCE in 0.1 mol/L PBS at pH 7.4 for (B)-(D) in presence of 0.1 mol/L TEA for (A) and (D). Error bars = SD (n = 3).

3.6. ECL efficiency upon Co^{2+} doping in AuNCs

The ECL efficiency (Φ_{ECL}) was examined using 1 mmol/L $Ru(bpy)_3^{2+}$/TPrA as the reference with following equation [40].

$$\Phi_{ECL} = \Phi^o_{ECL} (I / Q) / (I^o / Q^o) \quad (6)$$

where, Φ^o_{ECL} is the ECL efficiency of $Ru(bpy)_3^{2+}$/TprA and defined as 1 (Fig. S5), I and I^omean the relevant ECL response, and Q and Q^omean the consumed charges (integrating current and time), respectively.

In 0.1 mol/L pH 7.4 PBS containing 0.1 mol/L TEA, the ECL efficiency of Co^{2+}-AuNCs and AuNCs was measured to be 33.8% and 15.6%, respectively (Fig. S7B). Since the ECL intensity, efficiency and wavelength of AuNCs could be regulated by altering the surface stabilizers [22], the ECL efficiency of obtained AuNCs was almost 4 times that of ER-AuNCs/$S_2O_8^{2-}$ system. In addition, the ECL efficiency of Co^{2+}-AuNCs was 8.2 times higher than that of 4.11% for above ER-AuNCs/$S_2O_8^{2-}$ system [17], and was also much better than those of Mn@CdInS (2.1%) [41] and polyaniline-$[Ru(bpy)_2PIC]^{2+}$ (1.0%) [42]. The perfect efficiency of Co^{2+}-AuNCs indicated a significant and promising breakthrough for establishing a mechanistic framework to improve the ECL efficiency [17].

3.7. Feasibility of ECL immunosensing with Co^{2+}-AuNCs as tag

CV is an efficient and favorable method for observing the surface modification of the electrodes [43]. The fabrication and detection procedures of the immunosensor for NSE were demonstrated by Fe $(CN)_6^{3-}$/Fe$(CN)_6^{4-}$ redox couple in 0.1 mol/L pH 7.4 PBS. The GCE showed a pair of well-shaped redox peaks along with the peak separation (ΔEp) of 72 mV (Fig. S8A, curve a). When ABA was electrodeposited onto the GCE, the electrode displayed an obviously lower peak value and enhanced peak separation (Fig. S8A, curve b), which was owing to the electrostatic repulsion between the negatively charged Fe $(CN)_6^{3-}$/Fe$(CN)_6^{4-}$ and the surface of GCE=ABA (pKa of ABA is 4.80) [44]. After Ab_1 was covalently bound to GCE=ABA, the peak currents and the peak potential separation of Fe$(CN)_6^{3-}$/Fe$(CN)_6^{4-}$ were partially restored (Fig. S8A, curve c), which indicated that the negatively charged surface of GCE=ABA was partially changed due to the binding of Ab_1. Upon the capture of NSE and then Ab_2|Co^{2+}-AuNCs, the current responses decresed and the peak potential separation decreased again (Fig. S8A, curves d and e), indicating that the immunocomplexes hindered the electron transfer. According to the ECL curves, GCE=ABA-Ab_1 and its recognition to NSE did not showed any ECL response in 0.1 mol/L pH 7.4 PBS containing 0.1 mol/L TEA, and the immunosensor produced sensitive ECL response at + 0.95 V only after Ab_2|Co^{2+}-AuNCs were bound to its surface (Fig. S8B), supplying a sensitive and low-background strategy for ECL immunoassay of NSE. More importantly, Co^{2+}-AuNCs could maintain its excellent ECL radiation performance during the construction process. In addition, the atomic force microscopic (AFM) images demonstrated the loading of different layers on GCE, which changed the surface roughness, and the successful fabrication of the immunosensor (Fig. S9).

3.8. ECL immunosensing performance for NSE detection

In 0.1 mol/L pH 7.4 PBS containing 0.1 mol/L TEA, the sandwiched immunocomplex modified electrode showed greater ECL response with the increasing NSE content (Fig. 6A). The plot of the ECL intensity vs the logarithmic value of NSE content ranging from 0.0005 to 1000 pg/mL showed well linearity (R^2 =0.996) (Fig. 6B). The limit of detection (LOD) for the immunosnsor was 0.16 fg/mL at 3S/N. The linear concentration range was broader, and the LOD was lower than other reported ECL bioassays [45–49] (Table 1), indicating the excellent immunosensing performance.

The stability, reproducibility and selectivity were very significant for the analytical property of the immunosensor [10]. The obtained immunosensor possessed excellent operational stability with the relative standard deviation (RSD) of 1.1% for 11 circles scanning (Fig. 6C) [50]. Furthermore, the storage stability of immunosensor was also determined by placing the fabricated immunosensors for 20 days, which showed the ECL signal of 83% the original signal, demonstrating the excellent stability (Fig. 6D). The ECL responses of seven proposed immunosensors were firstly examined at 10 pg/mL NSE to demonstrate the excellent reproducibility of the immunosensor fabrication with the RSD of 1.3% (Fig. 6E). The immunosensor showed negligible response to α-fetoprotein (AFP), carcinoembryonic antigen (CEA), prostate specific antigen (PSA) and carcinoma antigen 125 (CA125) at the concentration 100 folds that of NSE (Fig. 6F). When they coexisted in NSE solution, the ECL signal did not any change compared with NSE alone. Thus the proposed ECL immunosensor for NSE possessed favorable selectivity.

3.9. Analysis of NSE in human serum samples

The acceptance of the strategy and the proposed immunosensor was further demonstrated by evaluating the actual results of the immunoassay for NSE in serum samples [51]. The standard addition method was applied to accomplish the corresponding detection [52]. The consequences were displayed in Table S1, which showed the RSD of less than 3.87%, and the recovery from 98.9% to 102.5%, demonstrating the potential application of the prepared strategy in clinical detection.

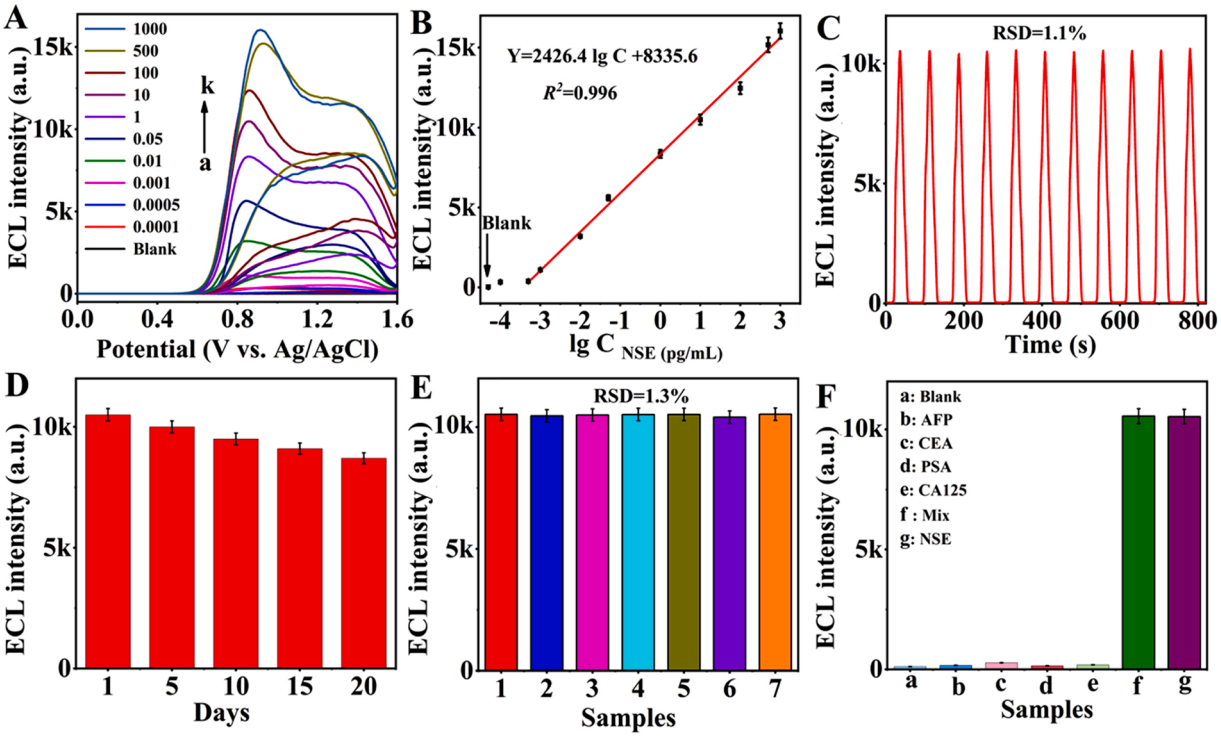

Fig. 6. . (A) ECL-potential curves of immunosensors in pH 7.4 PBS with 0.1 mol/L TEA at 50 mV/s at 0, 0.0001, 0.0005, 0.001, 0.01, 0.05, 1, 10, 100, 500 and 1000 pg/mL NSE (from a to k), (B) corresponding working curve for NSE detection, (C) operational stability under continuous scanning (11 circles), (D) positioned stability and (E) reproducibility of the immunosensor at 10 pg /mL NSE, and (F) selectivity of the immunosensor at 10 pg/mL NSE and 1 ng/mL other interferents.

Table 1
Comparison of ECL methods for NSE detection.

Immunocomplex	Methods	Line range (ng/mL)	LOD (pg/mL)	Triggering potential	ECL efficiency	Ref.
GCE/DMSA-CdTeQDs/Ab_1/NSE/HRP-SWCNHs-Ab_2	ECL	10^{-3}-10^{3}	0.44	-1.3 V		[45]
GCE/SnS_2NF@Pt/Ab_1/NSE/AuNRs-Ab_2	ECL	2×10^{-4}-20	0.079	-1.5 V		[46]
GCE/SCNWs-Ab_1/NSE/amino-rGO/N-CQDs-Ab_2	ECL	5.5×10^{-7}-5	1.8×10^{-4}			[47]
GCE/Ru-SiO_2 @PEI-Nafion-AuNPs-Ab/NSE	ECL	10^{-5}-10	10^{-2}			[48]
GCE/Pd-Cu_2O-NFC/Ab_1/NSE/ AgNCs-NFC-Ab_2	ECL	10^{-5}-100	3.65×10^{-2}			[49]
GCE/ABA-Ab_1/NSE/Co^{2+}-AuNCs-Ab_2	ECL	5×10^{-7}-1	1.6×10^{-4}	+ 0.95	33.8%	This work

4. Conclusion

By designing an ion doping strategy for promoting the radiative charge transfer and regulating the hole-injected channel of AuNCs, a NIR ECL luminophore with enhanced emission, lowered triggering potential and enhanced Φ_{ECL} has been obtained. The luminophore can be conveniently synthesized via Co^{2+} doping in AuNCs. Compared with AuNCs, the Co^{2+}-AuNCs show 0.2 V more negative anodic emission potential, double ECL intensity and much higher ECL efficiency, which lead to low background and high sensitivity for NIR ECL analysis. Thus a sensitive immunosensing method for NES detection has been proposed, which shows excellent immunosensing performance with wide concentration range, low LOD, excellent specificity and good practicability. The doping strategy offers a convenient way for modulating the ECL features of NCs-based luminophores and exploring novel ECL luminophores with admirable performance for bioassay. Further efforts will improve the ECL monochromaticity of Co^{2+}-AuNCs for spectrum-resolved multiplexing immunoassay and bioimaging.

CRediT authorship contribution statement

Hongying Jia: Conceptualization, Data curation, Writing – original draft. **Lei Yang:** Formal analysis. **Dawei Fan:** Review the data. **Xuan Kuang:** Editing the draft. **Xu Sun:** Editing the draft. **Qin Wei**: Funding acquisition, Project administration. **Huangxian Ju:** Funding acquisition, Project administration, Writing – review & editing.

Declaration of Competing Interest

The authors declare that they have no known competing financial interests or personal relationships that could have appeared to influence the work reported in this paper.

Acknowledgements

This project was supported by the National Natural Science Foundation of China (21627809, 21827812, 21890741), the Special Foundation for Taishan Scholar Professorship of Shandong Province (No. TS201712052) and the Innovation Team Project of Colleges and Universities in Jinan (No. 2019GXRC027).

Appendix A. Supporting information

Supplementary data associated with this article can be found in the online version at doi:10.1016/j.snb.2022.132034.

References

[1] N.N. Wang, Z.Y. Wang, L.Z. Chen, W.W. Chen, Y.W. Quan, Y.X. Cheng, H.X. Ju, Dual resonance energy transfer in triple-component polymer dots to enhance electrochemiluminescence for highly sensitive bioanalysis, Chem. Sci. 10 (2019) 6815–6820.
[2] X. Tan, B. Zhang, G.Z. Zou, Electrochemistry and electrochemiluminescence of organometal halide perovskite nanocrystals in aqueous medium, J. Am. Chem. Soc. 139 (2017) 8772–8776.
[3] C. Ma, H.F. Wei, M.X. Wang, S.J. Wu, Y.C. Chang, J.R. Zhang, et al., Hydrogen evolution reaction monitored by electrochemiluminescence blinking at single-nanoparticle level, Nano Lett. 20 (2020) 5008–5016.
[4] S. Chen, H.D. Ma, J.W. Padelford, W.L. Qinchen, W. Yu, S.X. Wang, et al., Near infrared electrochemiluminescence of rod-shape 25-atom AuAg nanoclusters that is hundreds-fold stronger than that of Ru(bpy)$_3$ standard, J. Am. Chem. Soc. 141 (2019) 9603–9609.
[5] Y.G. Wang, G.H. Zhao, H. Chi, S.H. Yang, Q.F. Niu, D. Wu, et al., Self-luminescent lanthanide metal-organic frameworks as signal probes in electrochemiluminescence immunoassay, J. Am. Chem. Soc. 143 (2021) 504–512.
[6] Q. Hua, F.Y. Tang, X.B. Wang, M. Li, X.W. Gu, W.J. Sun, et al., Electrochemiluminescence sensor based on EuS nanocrystals for ultrasensitive detection of mercury ions in seafood, Sens. Actuators B Chem. 352 (2022), 131075.
[7] Am Zhang, C.S. Huang, H.Y. Shi, W.W. Guo, X. Zhang, H.K. Xiang, et al., Electrochemiluminescence immunosensor for sensitive determination of tumor biomarker CEA based on multifunctionalized flower-like Au@BSA nanoparticles, Sens. Actuators B Chem. 238 (2017) 24–31.
[8] L. Fu, B. Zhang, K.N. Fu, X.W. Gao, G.Z. Zou, Electrochemically lighting up luminophores at similar low triggering potentials with mechanistic insights, Anal. Chem. 92 (2020) 6144–6149.
[9] L. Wang, M.H. Jiang, Y.Q. Chai, R. Yuan, Y. Zhuo, Intense electrochemiluminescence from an organic microcrystal accelerated H_2O_2-free luminol system for microRNA detection, Chem. Commun. 56 (2020) 9000–9003.
[10] X. Dong, Y. Du, G.H. Zhao, W. Cao, D.W. Fan, X. Kuang, et al., Dual-signal electrochemiluminescence immunosensor for neuron-specific enolase detection based on "dual-potential" emitter Ru(bpy)$_3^{2+}$ functionalized zinc-based metal-organic frameworks, Biosens. Bioelectron. 192 (2021), 113505.
[11] N.N. Wang, H. Gao, Y.Z. Li, G.M. Li, W.W. Chen, Z.C. Jin, et al., Dual intramolecular electron transfer for in situ coreactant-embedded electrochemiluminescence microimaging of membrane protein, Angew. Chem. Int. Ed. 59 (2020) 1–6.
[12] Y. He, S. Hou, L. Yang, F. Zhang, G. Zou, Adjustable electrochemiluminescence from highly passivated CdTe/CdS nanocrystals by simple surface decoration with counterions, Chem. Eur. J. 24 (2018) 9592–9597.
[13] M. Hesari, Z.F. Ding, A grand avenue to Au nanocluster electrochemiluminescence, Acc. Chem. Res. 50 (2017) 218–230.
[14] Y. Jia, L. Yang, J.W. Xue, N. Zhang, D.W. Fan, H.M. Ma, et al., Bioactivity-protected electrochemiluminescence biosensor using gold nanoclusters as the low-potential luminophor and Cu_2S snowflake as co-reaction accelerator for procalcitonin analysis, ACS Sens 4 (2019) 1909–1916.
[15] Y. Cheng, J.P. Lei, Y.L. Chen, H.X. Ju, Highly selective detection of microRNA based on distance-dependent electrochemiluminescence resonance energy transfer between CdTe nanocrystals and Au nanoclusters, Biosens. Bioelectron. 51 (2014) 431–436.
[16] H.P. Peng, M.L. Jian, Z.N. Huang, W.J. Wang, H.H. Deng, W.H. Wu, et al., Facile electrochemiluminescence sensing platform based on high-quantum-yield gold nanocluster probe for ultrasensitive glutathione detection, Biosens. Bioelectron. 105 (2018) 71–76.
[17] H.P. Peng, M.L. Jian, H.H. Deng, W.J. Wang, Z.N. Huang, K.Y. Huang, et al., Valence states effect on electrogenerated chemiluminescence of gold nanocluster, ACS Appl. Mater. Interfaces 9 (2017) 14929–14934.
[18] W.J. Miao, J.P. Choi, A.J. Bard, Electrogenerated chemiluminescence 69: The Tris (2,2′-bipyridine)ruthenium(II), (Ru(bpy)$_3^{2+}$)/Tri-*n*-propylamine (TPrA) system revisiteds a new route involving TPrA$^{\bullet+}$ cation radicals, J. Am. Chem. Soc. 124 (2002) 14478–14485.
[19] T. Wang, D. Wang, J.W. Padelford, J. Jiang, G. Wang, Near-infrared electrogenerated chemiluminescence from aqueous soluble lipoic acid Au nanoclusters, J. Am. Chem. Soc. 138 (2016) 6380–6383.
[20] H.P. Peng, Z.N. Huang, H.H. Deng, W.H. Wu, K.Y. Huang, Z.L. Li, et al., Dual enhancement of gold nanocluster electrochemiluminescence: electrocatalytic excitation and aggregation-induced emission, Angew. Chem. Int. Ed. 59 (2020) 9982–9985.
[21] L.Q. Yang, B. Zhang, L. Fu, K.N. Fu, G.Z. Zou, Efficient and monochromatic electrochemiluminescence of aqueous-soluble Au nanoclusters via host-guest recognition, Angew. Chem. Int. Ed. 58 (2019) 6901–6905.
[22] H.Y. Jia, S.Q. Yu, L. Yang, Q. Wei, H.X. Ju, Near-infrared electrochemiluminescence of dual-stabilizer-capped Au nanoclusters for immunoassays, ACS Appl. Nano Mater. 4 (2021) 2657–2663.
[23] J.B. Liu, R.S. Zhao, X. Wang, X.W. Gao, G.Z. Zou, Mechanistic investigations into synergistically enhanced radiative-charge-transfer in Au-Ag bimetallic nanoclusters, Chem. Commun. 56 (2020) 5665–5668.

[24] L.E. Marbella, C.M. Andolina, A.M. Smith, M.J. Hartmann, A.C. Dewar, K. A. Johnston, et al., Gold-cobalt nanoparticle alloys exhibiting tunable compositions, near-infrared emission, and high T_2 relaxivity, Adv. Funct. Mater. 24 (2014) 6532–6539.
[25] S.E. Crawford, M.J. Hartmann, J.E. Millstone, Surface chemistry-mediated near-infrared emission of small coinage metal nanoparticles, Acc. Chem. Res. 52 (2019) 695–703.
[26] B.J. Gao, M.A. Haghighatbin, H. Cui, Polymer-encapsulated cobalt/gold bimetallic nanoclusters as stimuli-responsive chemiluminescent nanoprobes for reactive oxygen species, Anal. Chem. 92 (2020) 10677–10685.
[27] C. Zhang, Z.F. Ma, PtCu nanoprobe-initiated cascade reaction modulated iodide-responsive sensing interface for improved electrochemical immunosensor of neuron-specific enolase, Biosens. Bioelectron. 143 (2019), 111612.
[28] X. Huang, J. Miao, J. Fang, X. Xu, Q. Wei, W. Cao, Ratiometric electrochemical immunosensor based on L-cysteine grafted ferrocene for detection of neuron specific enolase, Talanta 239 (2022), 123075.
[29] E.B. Aydın, M. Aydın, M.K. Sezgintürk, Selective and ultrasensitive electrochemical immunosensing of NSE cancer biomarker in human serum using epoxy-substituted poly(pyrrole) polymer modified disposable ITO electrode, Sens. Actuators B Chem. 306 (2020), 127613.
[30] H.H. Deng, K.Y. Huan, S.B. He, L.P. Xue, H.P. Peng, D.J. Zha, et al., Rational design of high-performance donor-linker-acceptor hybrids using a schiff base for enabling photoinduced electron transfer, Anal. Chem. 92 (2020) 2019–2026.
[31] X. Tan, B. Zhang, J. Zhou, G.Z. Zou, Spectrum-based electrochemiluminescence immunoassay for selectively determining CA125 in greenish waveband, ChemelectroChem 4 (2017) 1714–1718.
[32] W. van der Stam, M. de Graaf, S. Gudjonsdottir, J.J. Geuchies, J.J. Dijkema, N. Kirkwood, et al., Tuning and probing the distribution of Cu^{+} and Cu^{2+} trap states responsible for broad-band photoluminescence in $CuInS_2$ nanocrystals, ACS Nano 12 (2018) 11244–11253.
[33] X.F. Jiang, X.Y. Wang, C. Yao, S.X. Zhu, L. Liu, R.H. Liu, et al., Surface-engineered gold nanoclusters with biological assembly-amplified emission for multimode imaging, J. Phys. Chem. Lett. 10 (2019) 5237–5243.
[34] J.P. Xie, Y.G. Zheng, J.Y. Ying, Protein-directed synthesis of highly fluorescent gold nanoclusters, J. Am. Chem. Soc. 131 (2009) 888–889.
[35] G. Zhang, P. Wang, W.T. Lu, C.Y. Wang, Y.K. Li, C. Ding, et al., Co nanoparticles/Co, N, S tri-doped graphene templated from in-situ-formed Co, S Co-doped g-C_3N_4 as an active bifunctional electrocatalyst for overall water splitting, ACS Appl. Mater. Interfaces 9 (2017) 28566–28576.
[36] Z.T. Luo, X. Yuan, Y. Yu, Q.B. Zhang, D.T. Leong, J.Y. Lee, et al., From aggregation-induced emission of Au(I)-thiolate complexes to ultrabright Au(0)@Au(I)-thiolate core-shell nanoclusters, J. Am. Chem. Soc. 134 (2012) 16662–16670.
[37] Y.P. He, L.Q. Yang, F. Zhang, B. Zhang, G.Z. Zou, Tunable electron-injection channels of heterostructured ZnSe@CdTe nanocrystals for surface-chemistry-involved electrochemiluminescence, J. Phys. Chem. Lett. 9 (2018) 6089–6095.
[38] A.L. Lu, D.L. Peng, F.F. Chang, Z. Skeete, S.Y. Shan, A. Sharma, et al., Composition- and structure-tunable gold-cobalt nanoparticles and electrocatalytic synergy for oxygen evolution reaction, ACS Appl. Mater. Interfaces 8 (2016) 20082–20091.
[39] G. Valenti, E. Rampazzo, S. Kesarkar, D. Genovese, A. Fiorani, A. Zanut, et al., Electrogenerated chemiluminescence from metal complexes-based nanoparticles for highly sensitive sensors applications, Coord. Chem. Rev. 367 (2018) 65–81.
[40] M. Hesari, M.S. Workentin, Z.F. Ding, Highly efficient electrogenerated chemiluminescence of Au_{38} nanoclusters, ACS Nano 8 (2014) 8543–8553.
[41] F. Wang, J. Lin, T.B. Zhao, D.D. Hu, T. Wu, Y. Liu, Intrinsic "Vacancy Point Defect" induced electrochemiluminescence from coreless supertetrahedral chalcogenide nanocluster, J. Am. Chem. Soc. 138 (2016) 7718–7724.
[42] K.M. Molapo, A. Venkatanarayanan, C.M. Dolan, U. Prendergast, P.G. Baker, E. I. Iwuoha, et al., High efficiency electrochemiluminescence from polyaniline: ruthenium metal complex films, Electrochem. Commun. 48 (2014) 95–98.
[43] J.W. Xue, L. Yang, Y. Du, Y. Ren, X. Ren, H.M. Ma, et al., Electrochemiluminescence sensing platform based on functionalized poly-(styrene-co-maleicanhydride) nanocrystals and iron doped hydroxyapatite for CYFRA 21-1 immunoassay, Sens. Actuators B Chem. 321 (2020), 128454.
[44] X.W. Gao, K.N. Fu, L. Fu, H.S. Wang, B. Zhang, G.Z. Zou, Red-shifted electrochemiluminescence of CdTe nanocrystals via Co^{2+}-doping and its spectral sensing application in near-infrared region, Biosens. Bioelectron. 150 (2020), 111880.
[45] Y.L. Ai, X. Li, L. Zhang, W.Y. Zhong, J. Wang, Highly sensitive electrochemiluminescent immunoassay for neuron-specific enolase amplified by single-walled carbon nanohorns and enzymatic biocatalytic precipitation, J. Electroanal. Chem. 818 (2018) 257–264.
[46] G.C. Mo, X.M. He, D.M. Qin, X.H. Jiang, X.F. Zheng, B.Y. Deng, A potential-resolved electrochemiluminescence resonance energy transfer strategy for the simultaneous detection of neuron-specific enolase and the cytokeratin 19 fragment, Analyst 146 (2021) 1334–1339.
[47] X.F. Zheng, G.C. Mo, Y.Y. He, D.M. Qin, X.H. Jiang, W.M. Mo, et al., Electrochemiluminescent immunoassay for neuron specific enolase by using amino-modified reduced graphene oxide loaded with N-doped carbon quantum dots, Microchim. Acta 186 (2019) 817.
[48] L.M. Zhou, J.S. Huang, B. Yu, T.Y. You, A novel self-enhanced electrochemiluminescence immunosensor based on hollow Ru-SiO_2@PEI nanoparticles for NSE analysis, Sci. Rep. 6 (2016) 22234.
[49] X.Z. Song, T.T. Wu, C.N. Luo, L. Zhao, X. Ren, Y. Zhang, et al., Peptide-based electrochemiluminescence biosensors using silver nanoclusters as signal probes and Pd-Cu_2O hybrid nanoconcaves as coreactant promoters for immunoassays, Anal. Chem. (2021).
[50] X.Z. Song, X.R. Shao, L. Dai, D.W. Fan, X. Ren, X.J. Sun, et al., Triple amplification of 3,4,9,10-perylenetetracarboxylic acid by Co^{2+}-based metal-organic frameworks and silver-cysteine and its potential application for ultrasensitive assay of procalcitonin, ACS Appl. Mater. Interfaces 12 (2020) 9098–9106.
[51] E.H. Ma, P. Wang, Q.S. Yang, H.X. Yu, F.B. Pei, Y.T. Zheng, et al., Electrochemical immunosensors for sensitive detection of neuron-specific enolase based on small-size trimetallic Au@Pd^Pt nanocubes functionalized on ultrathin MnO_2 nanosheets as signal labels, ACS Biomater. Sci. Eng. 6 (2020) 1418–1427.
[52] M.L. Yola, N. Atar, N. Ozcan, A novel electrochemical lung cancer biomarker cytokeratin 19 fragment antigen 21-1 immunosensor based on Si_3N_4/MoS_2 incorporated MWCNTs and core–shell type magnetic nanoparticles, Nanoscale 13 (2021) 4660–4669.

Hongying Jia received her B.S. and M.S. degrees in University of Jinan in 2013 and 2015 respectively. She is currently a Ph.D.student in School of Chemistry and Chemical Engineering, University of Jinan. Her research interests include nanomaterials-based biosensors.

Lei Yang received his B.S. in University of Jinan in 2016. He is currently a Ph.D. student in School of Chemistry and Chemical Engineering, University of Jinan. His interests are in nanomaterials-based biosensors.

Dawei Fan received her Ph. D degree from Lanzhou Institute of Chemical Physics, Chinese Academy of Sciences. She is currently an associate professor at University of Jinan. Her main research interests include electrochemical sensors and photoelectrochemical sensors. She has published over 50 papers.

Xuan Kuang obtained her Ph.D. in Analytical Chemistry in 2015. Her research interests focus on metal organic materials and their application in electrochemical sensors, and fundamental electrochemical studies of energy storage devices and synthetic nanomotors.

Xu Sun received her Ph.D. in inorganic chemistry at University of Science and Technology of China (USTC). She is now working as an associate professor in School of Chemistry and Chemical Engineering in University of Jinan. Currently, her research interests focus on the design and fabrication of novel nanomaterials for the construction of energy-related devices.

Qin Wei, a professor and DSc, has devoted herself to analytical teaching and scientific research. Her main research interests are the determination of protein and nucleic acid by photometry and the electrochemical immunosensor preparation. She has published over one hundred articles on analysis, immunosensor and applied successfully for many research projects, such as Biomaterials, Adv. Funct. Mater., Biosens. Bioelectron., Sens. Actuators B: Chem., Talanta.

Huangxian Ju received his BS, MS and Ph.D. degrees from Nanjing University during 1982–1992. He was a postdoc in Montreal University (Canada) from 1996 to 1997 and a guest professor in three universities of Germany and Ireland in 1999–2000. He became an associate and full professor of Nanjing University in 1993 and 1999. He is currently the director of State Key Laboratory of Analytical Chemistry for Life Science. His research interests focus on analytical biochemistry, biosensing and molecular diagnosis. He has published 13 books and 790 papers in different journals with SCIE h-index of 100 (>38000 citations) and Google Scholar h-index of .110 (> 44000 citations).